Virologica Sinica 40 (2025) 793–803

Contents lists available at ScienceDirect

Virologica Sinica

journal homepage: www.keaipublishing.com/en/journals/virologica-sinica
www.virosin.org

Research Article

A safe and broad-spectrum SARS-CoV-2 mRNA vaccine with a new delivery system for *in-situ* expression

Weiyi Yu [a], Xianying Chen [b], Qiubing Chen [c], Peixuan Chen [a], Naizhang Liu [a], Yingjian Li [a], Xue Tan [a], Qiuhan Zhang [d], Yan Rao [b], Ming Guo [a], Zhixiang Huang [b], Xin Wang [a], Zhen Zhang [b], Wenjie Xiang [a], Yuzhen Zhang [a], Qianyun Liu [a], Hao Yin [c,e], Li Zhou [b,*], Yu Chen [a,*], Ke Lan [a,b,d,e,*]

[a] *State Key Laboratory of Virology and Biosafety, RNA Institute, College of Life Sciences, Wuhan University, Wuhan, 430072, China*
[b] *Institute for Vaccine Research at Animal Bio-safety Level III Laboratory, Wuhan University, Wuhan, 430071, China*
[c] *Departments of Urology and Laboratory Medicine, Frontier Science Center for Immunology and Metabolism, Medical Research Institute, Zhongnan Hospital of Wuhan University, Wuhan University, Wuhan, 430071, China*
[d] *Department of Infectious Diseases, Frontier Science Center for Immunology and Metabolism, Medical Research Institute, Zhongnan Hospital of Wuhan University, Wuhan University, Wuhan 430071, China*
[e] *Taikang Center for Life and Medical Sciences, Wuhan University, Wuhan 430071, China*

ARTICLE INFO

Keywords:
SARS-CoV-2
mRNA vaccine
Lipid nanoparticles

ABSTRACT

Since the outbreak of COVID-19 in late 2019, the cumulative number of confirmed cases worldwide has surpassed 778 million, and the number of deaths has exceeded 7 million, posing a significant threat to human life and health while inflicting enormous losses on the global economy. At the stage where sequential immunization is recommended, there is a pressing demand for mRNA vaccines that can be rapidly adapted to new sequences, are easy to industrialize, and exhibit high safety and effectiveness. We developed a lipid nanoparticle (LNP) system, designated as WNP, which facilitates essentially *in situ* expression at the injection site and results in lower levels of pro-inflammatory factors in the liver, thus enhancing its safety compared to liver-targeted alternatives. Furthermore, in light of the swiftly mutating characteristic of SARS-CoV-2, a study has used cross-lineage chimeras and mutation patch strategies to design an antigen that is highly immunogenic and can stimulate the production of a broad range of effective antibodies. Therefore, we used the same antigenic configuration of RBD including five key mutation sites (K417T, L452R, T478K, E484K, and N501Y) to achieve optimal broad-spectrum efficacy. Our results indicate that WNP can elicit a humoral immunity response that is as robust as that of SM-102, a stronger cellular immune response, and provide a certain protective effect. On top of that, WNP can be applied to the development of vaccines targeting other pathogens and will contribute to a quicker response to the spillovers of unknown mammalian viruses.

INTRODUCTION

Coronaviruses are single-stranded, positive-stranded RNA viruses that exhibit high mutability. They can infect a wide range of mammals, including humans, causing respiratory, gastrointestinal, and neurological diseases. Severe acute respiratory syndrome coronavirus 2 (SARS-CoV-2) is the seventh coronavirus identified to infect humans and the third highly pathogenic coronavirus (Chen et al., 2020). Since its emergence at the end of 2019, the total number of confirmed cases worldwide has surpassed 778 million, with deaths exceeding 7 million (https://covid19.who.int/). This virus poses a serious threat to public health and has resulted in substantial global economic losses (Chen, L. et al., 2020; Zhou et al., 2020; Zhu et al., 2020).

* Corresponding authors.
E-mail addresses: klan@whu.edu.cn (K. Lan), chenyu@whu.edu.cn (Y. Chen), zhouli_jerry@whu.edu.cn (L. Zhou).

https://doi.org/10.1016/j.virs.2025.09.001
Received 9 June 2025; Accepted 1 September 2025
Available online 4 September 2025
1995-820X/© 2025 The Authors. Publishing services by Elsevier B.V. on behalf of KeAi Communications Co. Ltd. This is an open access article under the CC BY-NC-ND license (http://creativecommons.org/licenses/by-nc-nd/4.0/).

The viral particles of coronaviruses are approximately spherical, with an average diameter ranging from 118 to 136 nm. Among the four structural proteins, the spike (S) glycoprotein, the envelope (E) glycoprotein, and the membrane (M) glycoprotein are located on the viral envelope, whereas the nucleocapsid (N) phosphoprotein binds to RNA within the virus (Chen Y. et al., 2020b). The S protein of SARS-CoV-2 exists as a trimer with each monomer comprising S1 and S2 subunits. The receptor binding domain (RBD) within the S1 subunit interacts with angiotensin-converting enzyme 2 (ACE2) on the surface of the host cell, mediating the critical initial step of the infection (Wrapp et al., 2020).

Due to their large size and negative charge, mRNA molecules encounter difficulties in passively crossing negatively charged cell membranes. Furthermore, RNases in the blood and tissues will rapidly degrade RNA, triggering an innate immune response. Nevertheless, the innovations in synthesis, modification and delivery technologies have tackled the challenges related to high immunogenicity, low stability, vulnerability to degradation, and inefficient cellular uptake of mRNAs. In addition, RNA drug delivery systems based on lipids, polymers, dendrimer molecules and natural membranes have been developed, which can enable the delivery of RNA to target cells (Paunovska et al., 2022). The first Food and Drug Administration (FDA)-approved siRNA therapeutic, Onpattro, utilized MC3 and other lipids to successfully deliver siRNA to the liver (Zatsepin et al., 2016). Remarkably, less than two months after the onset of the pandemic, human SARS-CoV-2 mRNA vaccines were produced, which have been considered "a major technological leap in the history of vaccines". The first two FDA-approved mRNA vaccines, mRNA-1273 and BNT162b2, could deliver mRNA encoding antigenic sequences to target cells, thereby preventing SARS-CoV-2 infection. These vaccines employ the ionizable lipids SM-102 and ALC-0315, respectively (Dipiazza et al., 2021; Vogel et al., 2021). They have saved countless lives, reduced the severity of illness, and facilitated a return to normal life.

Typically, most vaccine recipients experience minimal discomfort, with only a few reporting mild self-limiting symptoms like fever, headache, and fatigue, or experiencing redness and swelling at the vaccination site (Meo et al., 2021). Serious adverse reactions, including allergic reactions, thrombotic thrombocytopenia syndrome, myocarditis, pericarditis, and Guillain-Barre syndrome, are extremely rare (Klein et al., 2021). Nonetheless, multiple cases of autoimmune hepatitis (AIH) have been reported following the administration of BNT162b2 or mRNA-1273 (Kim et al., 2023). Despite this, research has indicated that lipid nanoparticles (LNPs) free of mRNA do not result in liver injury (Tanaka et al., 2021). This suggests that off-target expression of the delivered mRNA may underlie safety concerns associated with mRNA vaccines.

Consequently, it is essential to develop LNPs that can deliver mRNA specifically to muscle tissues in order to reduce off-target effects and address safety concerns associated with current LNP formulations. This requires optimization of multiple factors. Critically, the proton dissociation constant (pKa) of the ionizable lipids governs both the tissue targeting precision and nucleic acid transfection efficacy of LNPs, with these parameters demonstrating a complex interdependence (Hassett et al., 2019; Carrasco et al., 2021; Chen, J. et al., 2023). In addition, the asymmetric tail structure helps to disrupt the endosomal membrane structure and can improve the transfection efficiency (Ali et al., 1998). To address these requirements, we have developed a delivery system that features an ionizable lipid with novel structural properties, appropriate nitrogen-phosphorus (N:P) ratio, carefully selected phospholipid type and molar ratio, and molar ratio of PEG lipids, etc.

The mRNA vaccines BNT162b2 and mRNA-1273 were created at the onset of the COVID-19 pandemic and showed effectiveness exceeding 90% during the early phases of the outbreak (Meo et al., 2021). Nonetheless, the protective efficacy of early vaccines against new infections has considerably waned. This decline is primarily driven by the continuous emergence of variants of SARS-CoV-2 carrying mutations, especially in the S protein, the main antigenic targets of mRNA vaccines. Mutations within the RBD may enhance its binding affinity to ACE2, potentially increasing the transmissibility or pathogenicity of the virus. On the other hand, these mutations may also modify critical epitopes of the antigen, enabling immune evasion (Chen, Y. et al., 2022). In addition, vaccine-induced neutralizing antibodies stimulated by vaccines, vital in combating the virus, generally decrease over time. Consequently, timely countermeasures are essential to enhance the effectiveness of vaccinations and reduce the incidence of severe illness and mortality.

Furthermore, original antigenic sin (OAS) refers to the immune memory generated when the immune system first encounters a specific pathogen, which subsequently influences the immune response to later pathogens that are similar to the initial one. The humoral immune imprint formed in the population through vaccination with the original wild-type vaccine or infection with the earliest wild-type SARS-CoV-2 can impair subsequent humoral immune responses to Omicron-specific vaccines (Aguilar-Bretones et al., 2023). Fortunately, a second Omicron spike booster can overcome this limitation, eliciting Omicron-neutralizing antibody titers comparable to primary immunization with the Omicron spike antigen (Yisimayi et al., 2024). Additionally, a leveraged vaccination strategy selecting antigens with maximal antigenic distance has been proposed to mitigate OAS and broaden neutralizing antibody responses (Zhang, G. et al., 2025).

Considering that the direct use of full-length S protein as the antigen has a high requirement for post-translational modification because of its long sequence (Kapoor et al., 2022), employing the RBD presents a more practical alternative. This approach circumvents challenges related to S protein conformation and modification while preserving immunogenicity. Besides, we connected the RBD to the hinge region (C_H2+C_H3) of the constant region (hFc) of human IgG1 antibodies. This design facilitates the formation of a dimer upon expression, enhancing the immunogenicity of the vaccine and prolonging its half-life *in vivo* (Sun et al., 2021).

In our prior research, COVID-19 convalescents from Wuhan exhibited a drastic decline in serum neutralization against the SARS-CoV-2 Omicron variants (Ma et al., 2022). Nevertheless, from a subset of convalescent sera demonstrating potent anti-Omicron activity, we successfully isolated broadly neutralizing antibodies (Liu et al., 2023). Furthermore, there is a limited difference in the immunogenic effects of using the Omicron sequence as an immunogen compared to the WT sequence (Ying et al., 2022). On the other hand, SARS-CoV-2 demonstrates convergent evolution, with mutations clustering at sites modulating ACE2-binding affinity and immune evasion (Cao et al., 2023; Zhao et al., 2023). This supports the strategic use of key mutation hotspots in antigen design. For instance, cross-lineage chimeras and mutation patch strategies have generated an antigen that is highly immunogenic and can stimulate the production of a broad range of effective antibodies (Wu et al., 2022). Therefore, we used the same antigenic configuration of RBD including five key mutation sites (K417T, L452R, T478K, E484K, and N501Y).

As sequential immunization is recommended, there is an increasing demand for mRNA vaccines that can be swiftly adapted to new sequences, are suitable for large-scale production, and ensure high levels of safety and effectiveness. Utilizing our designed cationic lipid and the sequence of RBD(M5)-hFc, our vaccine induced strong humoral and cellular immune responses in mice and conferred significant protection against SARS-CoV-2 challenge.

RESULTS

WNP can help form nanoparticles with physical characteristics similar to commercial systems and good *in vitro* delivery efficiency

To accommodate the structure of newly developed ionizable lipids and promote mRNA expression at the injection site, we adjusted the

traditional ratio of four lipids to formulate WNP (Fig. 1A). LNPs produced by a microfluidic device were filtered through an ultrafiltration centrifuge tube with continuous renewal of phosphate-buffered saline (PBS) and finally through a 0.22 μm filter membrane. In one experiment, the hydration diameter of SM-102 was recorded at 94.88 nm, while MC3 measured 78.14 nm, and WNP had a diameter of 69.29 nm (Fig. 1B). The transmission electron microscope (TEM) images (Fig. 1B) alongside the polydispersity index (PDI) suggested that the samples were nearly monodisperse (Fig. 1C). The zeta potential of SM-102, MC3 and WNP was observed to be approximately neutral (Fig. 1D), which helps to reduce potential cytotoxicity at physiological pH. Their encapsulation rates were around 95% (Fig. 1E). These results demonstrate that the particles made from WNP have similar physical properties to commercial lipids.

To assess the *in vitro* delivery efficiency of LNPs utilizing different systems, we transfected HEK 293T cells with luciferase-encapsulated LNPs. Luciferase expression (measured by relative light units, RLU) in cells treated with WNP-formulated LNP was comparable to that of SM-102 and significantly higher than that of MC3 (Fig. 1F). These results demonstrate the superior *in vitro* delivery capacity of the WNP system.

WNP enables localized mRNA expression at the injection site while demonstrating high delivery efficiency

To evaluate the *in vivo* delivery efficiency, we injected LNPs containing luciferase mRNA into mice. Six hours post injection, luminescence was detected in the muscle, liver and spleen of mice treated with the SM-102 system, while luminescence was observed only in the muscle and liver of those receiving MC3. In contrast, mice injected with WNP-injected mice revealed a notable signal restricted to the injection site (Fig. 2A and B). The total luminescent flux of WNP was significantly greater than that of the MC3 system at 6 and 24 h post injection. It was slightly lower than the luminescence from the SM-102 system at both 6 h and 48 h, and no significant difference was noted at 24 h (Fig. 2C). These results indicate that WNP exhibits commendable delivery efficiency, primarily concentrating at the injection site with limited expression in other organs (Fig. 2D).

The proteins translated from RBD(M5)-hFc mRNA can stably form dimers in cells

We have established a comprehensive platform for mRNA vaccine creation. We select RBD spanning residues 319–524 as the antigen, incorporating five mutation sites (K417N, L452R, T478K, E484K, N501Y) to achieve an optimal broad spectrum (Fig. 3A). The molecular weight of hFc monomer was approximately 26.3 kDa and that of RBD was about 23.6 kDa. RBD(M5)-hFc mRNA was transfected into HEK 293T cells, and the non-reducing sample band was detected in the 100–130 kDa range (Fig. 3B), which exceeds the combined weight of the two monomers. This discrepancy is likely due to glycosylation modification and implies that the RBD(M5)-hFc secreted into the supernatant successfully preserved its dimeric structure.

WNP has a good safety profile

To evaluate the safety of the vaccine, we administered RBD(M5)-hFc mRNA delivered in different formulations to mice on days 0 and 14. We then assessed the changes in serum glutamic-pyruvic transaminase (ALT) activity at 8 h after each injection, referencing the levels measured 7 days before the initial injection (Fig. 3C). The mice receiving WNP and SM-102 did not show a statistically significant increase in ALT activity compared to the placebo group 8 h after either injection (Fig. 3D). Furthermore, 8 h following the second injection, the mRNA levels of pro-inflammatory cytokines *Il1b*, *Tnfa* and *Il6* in the livers of mice treated with WNP did not significantly differ from those in the placebo group. However, the *Tnfa* levels in the SM-102 group were elevated compared to the placebo group (Fig. 3E). Hematoxylin and eosin (H&E) staining results indicated no

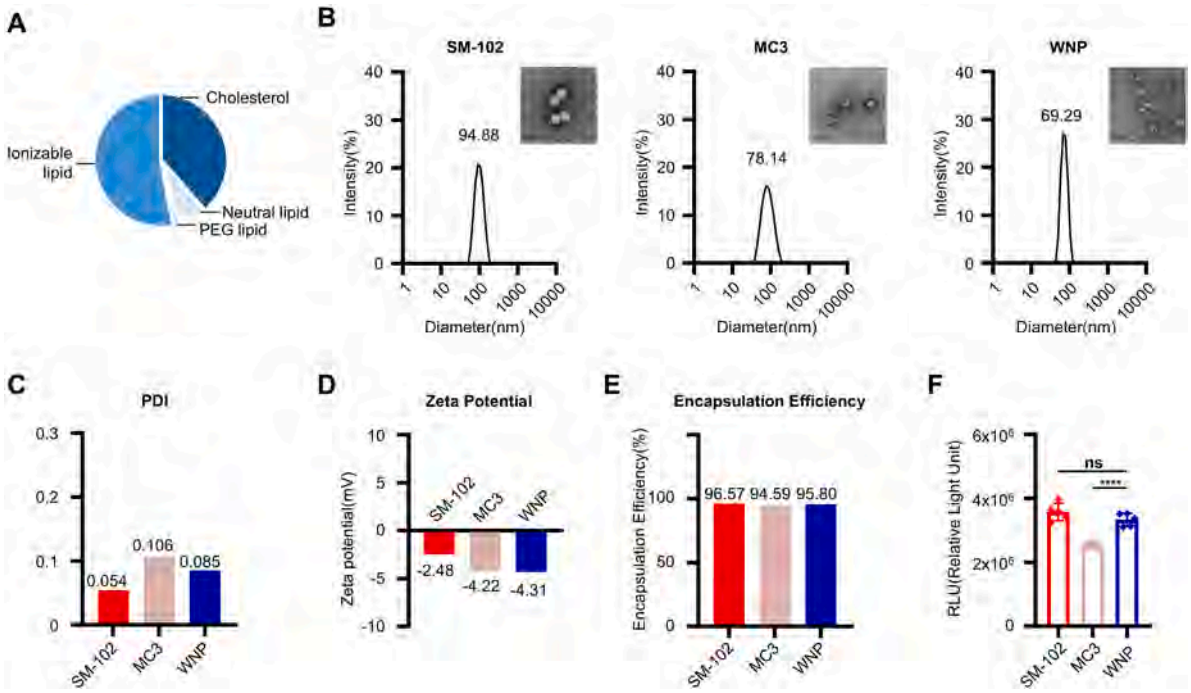

Fig. 1. Representative characterizations and *in vitro* delivery of WNP and other delivery systems.
A Schematic diagram of the formulation of WNP. **B** Representative size distribution and TEM images of SM-102, MC3 and WNP. **C, D, E** Representative polydispersity index (PDI), zeta potential and encapsulation efficiency of different delivery systems. **F** The delivery efficiency of WNP and other delivery systems in HEK 293T cells. Data are shown as mean ± SEM and analyzed by one-way ANOVA with multiple comparisons tests (ns, not significant, ****$P < 0.0001$).

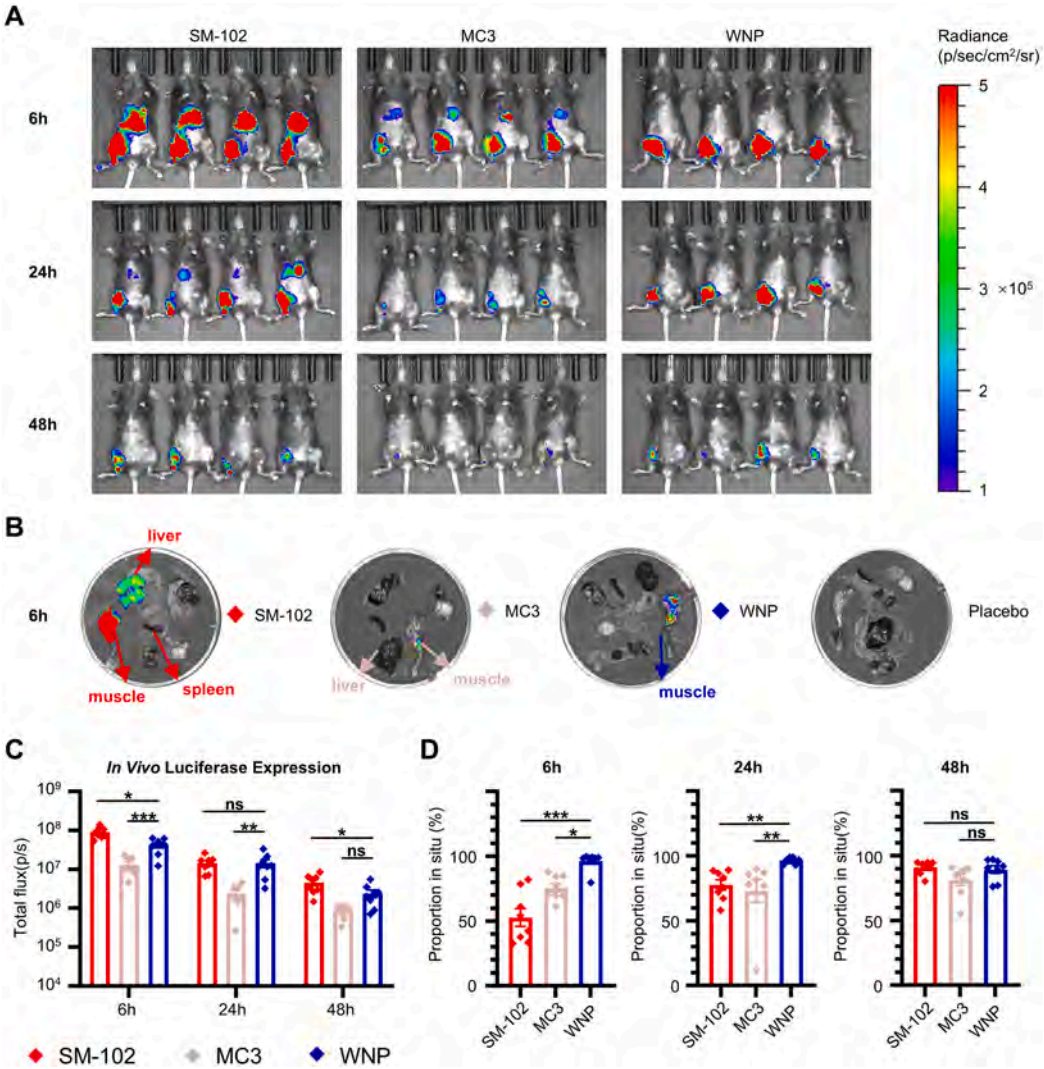

Fig. 2. *In vivo* delivery of WNP and other delivery systems.
A Representative bioluminescent images of female C57BL/6 mice after injection of different LNPs which encapsulated firefly luciferase mRNA. **B** Tissue distribution of reporter mRNA-LNP in mice, with mice injected placebo as a negative control. **C** The total luminous flux of the mice. **D** The proportions of the luminous flux between the injection site and other locations. Data are shown as mean ± SEM and analyzed by one-way ANOVA with multiple comparisons tests (ns, not significant, $^{*}P < 0.05$, $^{**}P < 0.01$, $^{***}P < 0.001$).

observable lesions in the liver or muscles of the mice across both groups (Fig. 3F). These results imply that the WNP system elicited a slightly milder inflammatory response relative to the SM-102 system.

WNP can elicit robust humoral and cellular immunity responses in mice

To evaluate the effectiveness of the vaccine, we administered LNP containing 1 μg of RBD(M5)-hFc mRNA to different groups of mice on days 0 and 14, followed by measuring the RBD(WT)-specific IgG levels in serum samples on days 14 and 28 (Fig. 4A). Our analysis revealed no significant difference in the RBD(WT)-specific antibody levels between the SM-102 and WNP formulations, with both eliciting robust RBD(WT)-specific antibody responses after the booster immunization (Fig. 4B). Additionally, serum samples collected on day 28 were also tested for their ability to inhibit the entry of pseudoviruses of Omicron variants BA.1, BA.5, BF.7, BQ.1.1, XBB.1.5, EG.5.2, JN.1 and KP.3. When compared to the placebo (PBS) group, the immunized groups exhibited significantly higher inhibition rates against various mutant pseudoviruses. The 50% pseudovirus neutralization titers ($PVNT_{50}$) against BA.1 were comparable between the WNP and SM-102 groups (Supplementary Fig. S1). In general, the inhibition rates showed no significant variation between the SM-102 and WNP groups (Fig. 4C).

On day 42, splenocytes were isolated and stimulated with Omicron BA.2 RBD-His protein. The ratios of IFN-γ, IL-2, IL-4, and IL-5 in $CD4^{+}$ T cells, along with those in $CD8^{+}$ cells, were markedly elevated in the WNP group when compared to the placebo group. In contrast, the proportions of cytokine-secreting cells (IFN-γ, IL-2, IL-4, IL-5) in the $CD4^{+}$ T cells from mice in the SM-102 group did not differ significantly from those in the WNP group. Notably, the $CD4^{+}$ T cells in the WNP group that produced IFN-γ, IL-2 and IL-4 were observed at higher levels than those in the SM-102 group, whereas IL-5 levels showed no significant difference. In summary, T cells exhibited enhanced secretion of Th1-associated cytokines (Fig. 4D).

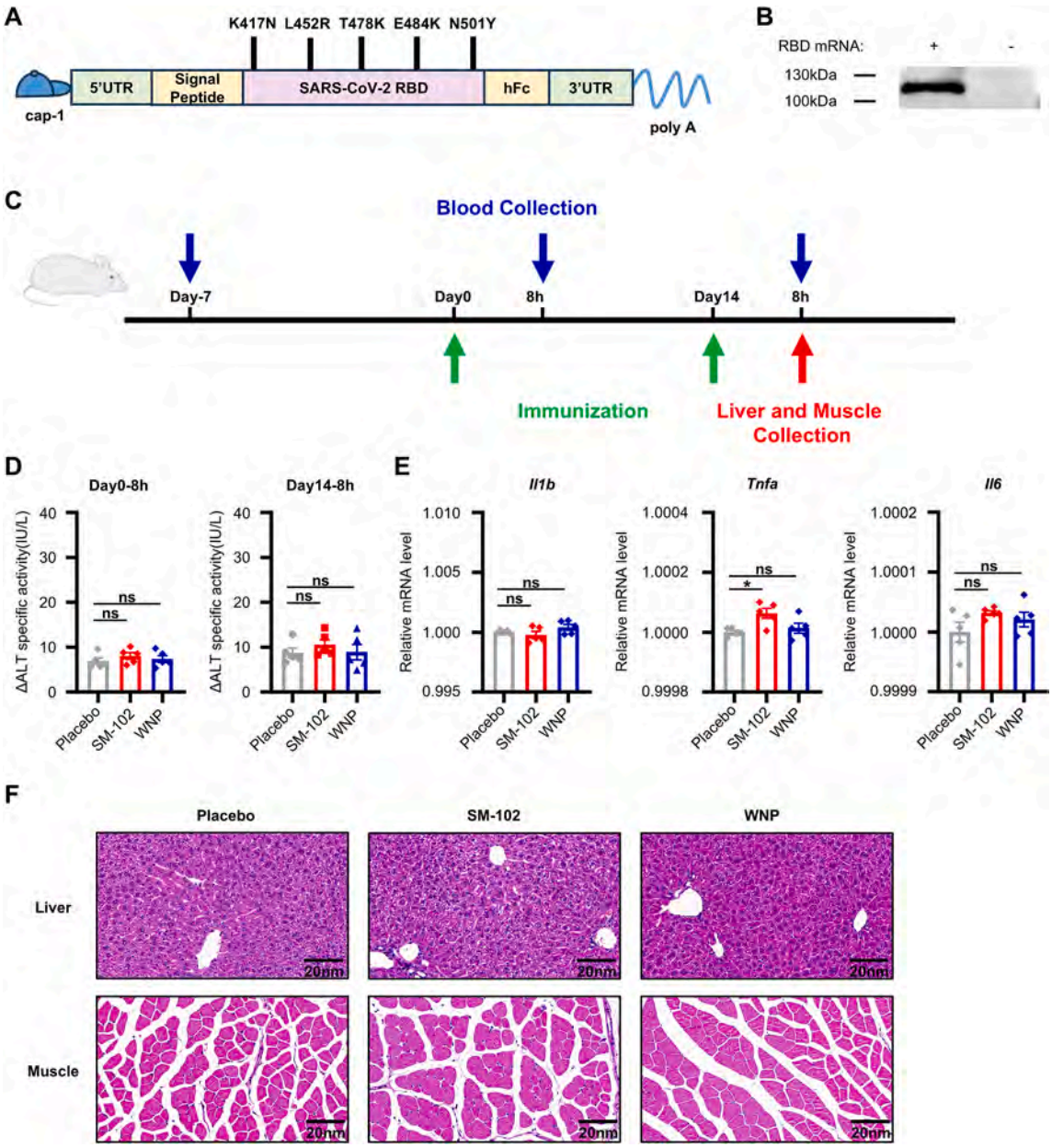

Fig. 3. Design of SARS-CoV-2 RBD(M5)-hFc mRNA and safety evaluation of WNP

Female BALB/c mice were intramuscularly injected with PBS (as negative control) or 1 μg RBD(M5)-hFc mRNA in SM-102 or in WNP at day 0 and day 14. Serum was collected at 7 days prior to the first injection and 8 h post every injection. Livers and muscles were collected 8 h after the second injection. **A** Schematic of SARS-CoV-2 RBD(M5)-hFc mRNA. **B** RBD(M5)-hFc protein expression from mRNA in HEK 293T cells. The mRNA was transfected into cells and the supernatant was detected after 48 h of culture. **C** Timeline of injection and sample collection. **D** The changes of activity of glutamic-pyruvic transaminase in serum. **E** The mRNA levels of proinflammatory cytokines *Il1b/Tnfa/Il6* in liver. **F** Representative pictures of H&E staining of livers and muscles. Data are shown as mean ± SEM and analyzed by one-way ANOVA with multiple comparisons tests (ns, not significant, $^{*}P < 0.05$, $^{**}P < 0.01$, $^{***}P < 0.001$, $^{****}P < 0.0001$).

WNP can provide protection for mice

To evaluate the protective efficacy of the vaccine, mice were infected with 43,500 plaque-forming unit (PFU) of Omicron BA.1 virus intranasally on day 35 and were subsequently euthanized at 4 dpi. The results indicated that administering the vaccine twice significantly reduced the copy number of viral genes present in the lungs, with no significant difference between the SM-102 and WNP groups (Fig. 5A). Pathological analysis displayed severe infiltration of inflammatory cells, thickening of alveolar walls, and some hemorrhagic points in the lungs of the placebo group, while the immunized group exhibited reduced lung damage. The injury scores for the SM-102 group were similar to those of the WNP group (Fig. 5B and C).

In addition, a replicon is a non-infectious, self-replicating RNA molecule that lacks viral structural genes but retains genes required for replication. When introduced into cells expressing complementary structural proteins, it enables efficient virion assembly. The system can be manipulated in a BSL-2 laboratory (Li et al., 2024). To evaluate the vaccine efficacy, we employed XBB.1.5-ΔN-GFP replicon delivery particles (RDPs) which can replicate in Caco-2-N cells. Sera from vaccinated mice can potently inhibit the replication of XBB.1.5 replicon virus

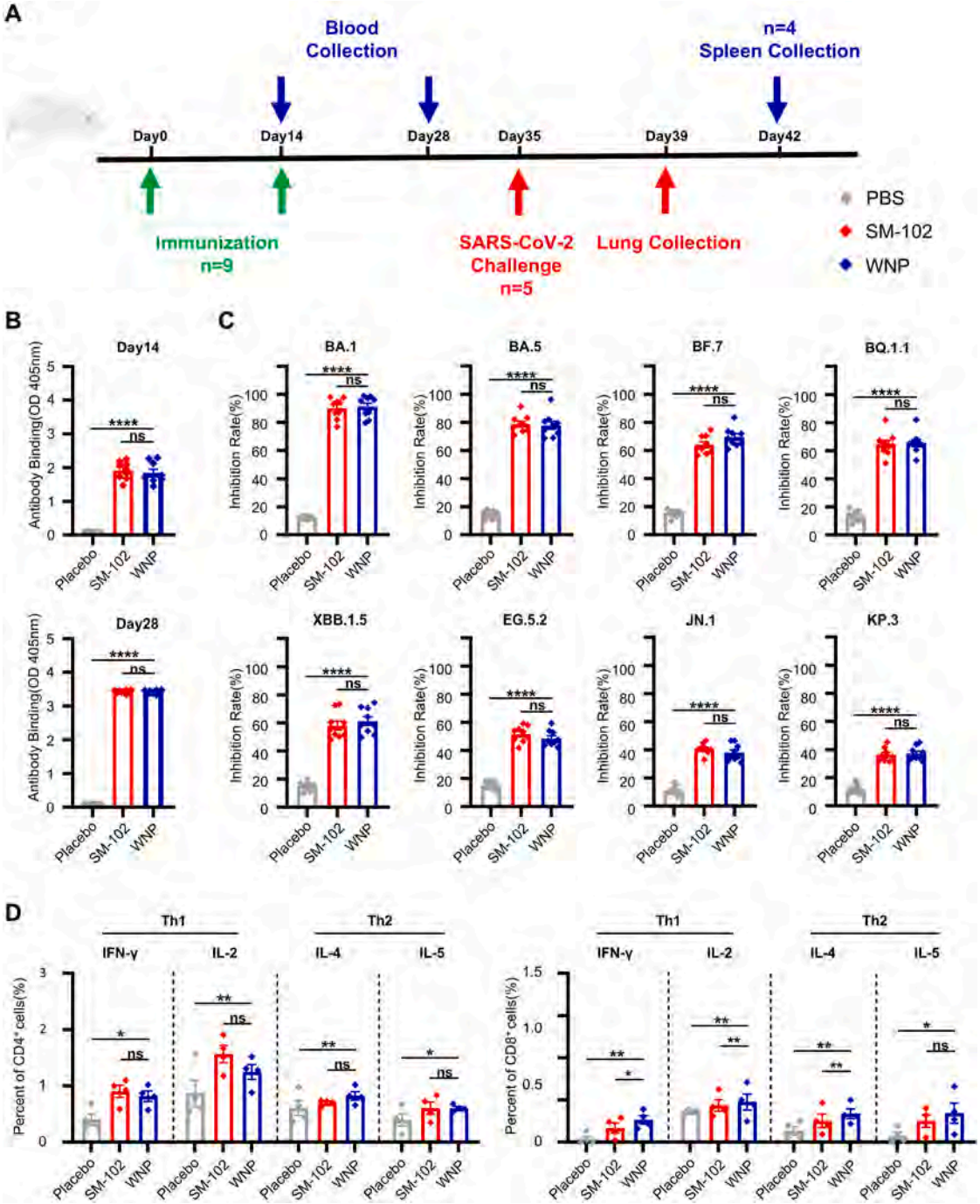

Fig. 4. Comparation of humoral immune responses and cellular immune responses triggered by different mRNA vaccines in mice.
Female BALB/c mice were intramuscularly injected with Placebo or 1 μg RBD(M5)-hFc mRNA in SM-102 or WNP (n = 9) at day 0 and day 14. Serum was collected at day 14 and day 28. Part of each group (n = 5) were infected with 43,500 PFU Omicron BA.1 and their lungs were collected 4 days post infection for viral load measurement and pathology analysis. The spleens of the residual mice were collected at day 42 for cellular immune response detection. **A** Timeline of immunization, challenge and sample collection. **B** The level of RBD(WT)-specific IgG in serum sapmles collected at day 14 and 28 after vaccination was demonstrated as optical density in ELISA. **C** The inhibition rates of serum sapmles collected on day 28 against BA.1, BA.5, BF.7, BQ.1.1, XBB.1.5, EG.5.2, JN.1 and KP.3 pseudoviruses ($TCID_{50}$ = 5000). **D** On day 42, RBD(BA.2)-specific IFN-γ, IL-2, IL-4 and IL-5 cells in $CD4^+$ and $CD8^+$ T cells in splenocytes were detected by flow cytometry. Data are shown as mean ± SEM and analyzed by one-way ANOVA with multiple comparisons tests (ns, not significant, $^*P < 0.05$, $^{**}P < 0.01$, $^{***}P < 0.001$).

particles, and there was no significant difference between the WNP group and the SM-102 group (Fig. 6A and B).

DISCUSSION

mRNA vaccines present several advantages, such as the ability to quickly adapt sequences, compatibility with industrial-scale production, and a high level of safety and effectiveness. These characteristics make them crucial in the post-epidemic period when sequential immunization is advised. However, many SARS-CoV-2 mRNA vaccines tend to accumulate in the liver (Zhang et al., 2020; Ai et al., 2023; Zheng et al., 2025), and the expression at non-target sites is a possible cause of side effects. In addition, since the virus mutates rapidly, how to design antigens to enable vaccines to have

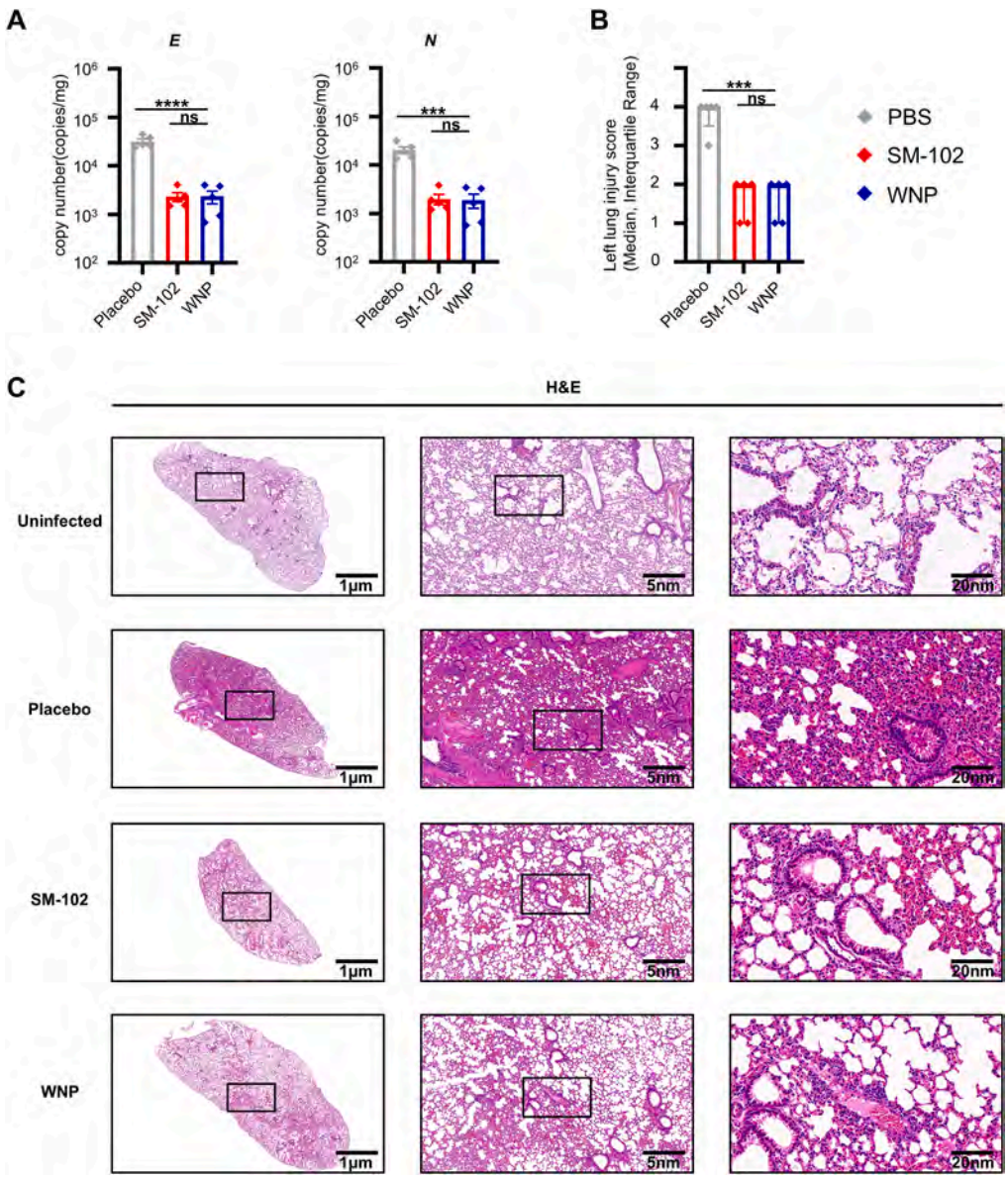

Fig. 5. Comparation of protective efficacy against Omicron BA.1 triggered by different mRNA vaccines.
A SARS-CoV-2 *N* and *E* gene copies number in the lungs. Data are shown as mean ± SEM and analyzed by one-way ANOVA with multiple comparisons tests (ns, not significant, $^{***}P < 0.001$, $^{****}P < 0.0001$). **B** Left pulmonary injury scores. Data are shown in median with interquartile range. Data are shown as mean with interquartile range and analyzed by Kruskal-Wallis test and Dunnett T3 post-test (ns, not significant, $^{****}P < 0.0001$). **C** Representative pictures of H&E staining of left lungs.

broad spectrum and long-term protection is also a direction that has been under ongoing exploration.

In this research, we conducted a comprehensive evaluation of a novel SARS-CoV-2 vaccine utilizing an in-house developed delivery system, WNP, including its immunogenicity, efficacy, and safety.

Throughout the development of the new LNP system, we designed the structure of the ionizable lipid and optimized the proportions of the four lipid components. *In vivo* imaging results showed that the mRNA delivered by our WNP demonstrated localized expression, while that delivered by SM-102 was primarily expressed in the liver 6 h post injection. We expect that the WNP administered into the body will display an increased utilization rate and invoke a lighter inflammatory response compared to SM-102.

Administering two doses of 1 μg of the vaccine to mice resulted in a strong humoral immune response, as shown by elevated levels of IgG and neutralizing antibodies. The results further proved that the antigen we chose can effectively induce the production of neutralizing antibodies against various mutant strains. Moreover, WNP can elicit a humoral immunity response that is as robust as that of SM-102 and a stronger cellular immune response. The vaccine stimulated immune responses that were characterized by Th1-biased $CD4^+$ T cells and $CD8^+$ cytotoxic T cells against the Omicron BA.2 variants. Finally, our vaccine provided a protective effect against Omicron BA.1 and XBB.1.5 variants. Combining the immune levels with the results of challenge experiments, we speculate that the vaccine could provide a broad spectrum of protection.

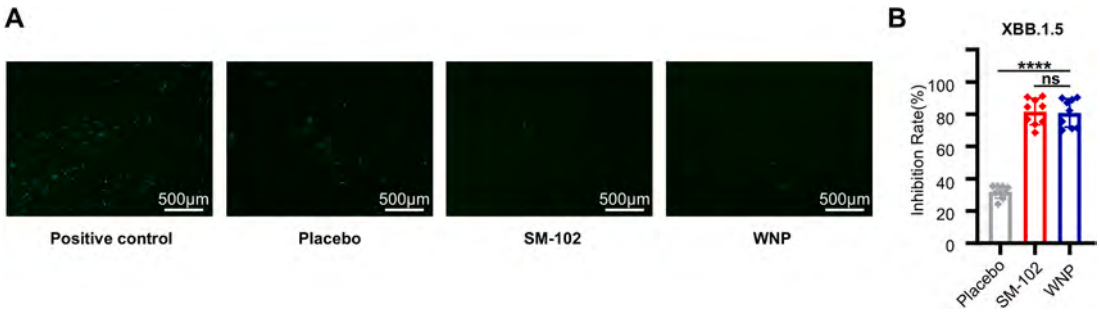

Fig. 6. Comparation of protective efficacy against XBB.1.5-ΔN-GFP replicon delivery particles triggered by different mRNA vaccines.
A Representative pictures of the infected cells by fluorescence microscope. **B** The inhibition rates of XBB.1.5 RDP of serum. Data are shown as mean ± SEM and analyzed by one-way ANOVA with multiple comparisons tests (ns, not significant, ****$P < 0.0001$).

In May 2023, the World Health Organization (WHO) announced that the outbreak of SARS-CoV-2 was no longer deemed a public health emergency of international concern (https://covid19.who.int/). The influence of SARS-CoV-2 on numerous countries worldwide is diminishing, yet the virus persists in mutating and spreading. Individuals continue to encounter the possibility of recurrent infections and severe cases. While vaccination has afforded a degree of protection, regrettably, this protective effect does not achieve the long-lasting immunity that many had hoped for. Respiratory illnesses typically surge during colder months. It is unusual to observe such a high rate of transmission of the novel coronavirus during the summer in the northern hemisphere. Current data indicates that climate has a minimal effect on the spread of the virus, showcasing a lack of significant seasonality. Consequently, it is possible that throughout the year, there may be periods of increased infections. The pandemic has persisted over time, still requiring our vigilance.

Numerous studies indicate that vaccination can considerably lower the likelihood of developing COVID-19 following infection and may also alleviate the severity of the disease (Lok et al., 2024). Nonetheless, the ongoing mutations of the virus present obstacles to vaccine efficacy. Changes in the sequence are still being continuously monitored. Since mRNA vaccine is effective and can be adjusted according to the sequences of the current strains in short order, it can provide protection for those at higher risk of severe illness (such as the elderly with reduced immunity) and also reduce the likelihood and severity of long COVID.

Although numerous newly developed and repurposed antiviral drugs have been applied in the treatment of COVID-19, most of them demonstrate suboptimal clinical efficacy. This underscores the urgent need for broader-spectrum antivirals with improved efficacy and safety profiles. Given that host-targeting agents carry higher risks of adverse events, prioritizing evolutionarily conserved viral targets—such as the HR1 domain, 3CL protease (3CLpro), and RNA-dependent RNA polymerase (RdRp)—represents a strategic approach to combat diverse SARS-CoV-2 variants and related coronaviruses (Lan et al., 2024). The E protein is another promising target, but its therapeutic utilization has been limited by inadequate inhibitors and effective screening methods. Notably, recent methodological advances in E ion channel screening now enable systematic discovery of novel candidates targeting this essential viral component. (Zhang, H. et al., 2025).

mRNA therapy presents considerable promise for both treating and preventing a range of diseases. With advancements in RNA modification technology, the stability, specificity and safety of RNA therapies are expected to improve substantially. We are currently looking for untranslated regions that demonstrate high translation capabilities and exploring methods to enhance their efficiency. Furthermore, we are investigating and refining several factors that influence the safety and effectiveness of delivery vectors. The system we established is anticipated to be applied to the research and development of vaccines targeting other pathogens. Additionally, it will contribute to a quicker response to the spillovers of unknown mammalian viruses (Shi, 2020).

In situ-expressed mRNA vaccines represent a promising therapeutic strategy against solid tumors, offering potential for tumor eradication and metastasis prevention. Their precise targeting capabilities can minimize the damage to normal tissues while directly eliciting a robust immune response within the tumor microenvironment. A muscle-specific isoform of the AB11B5C1 lipid nanoparticle has demonstrated potent anti-melanoma activity, significantly inhibiting tumor growth, enhancing antigen-specific $CD8^+$ T cell responses, and promoting substantial $CD8^+$ T cell infiltration into the tumor (Chen, J. et al., 2023). Additionally, studies have explored the use of mRNA vaccines to reprogram tumor cells, enabling their recognition and destruction by ovalbumin (OVA)-specific cytotoxic T lymphocytes, thereby markedly suppressing tumor growth across three murine subcutaneous solid tumor models and also effectively reprogramming the immunosuppressive tumor microenvironment, shifting it toward a more pro-inflammatory state (Fu et al., 2025).

CONCLUSIONS

Our developed delivery system, WNP, enables localized mRNA expression at the injection site. A novel SARS-CoV-2 vaccine utilizing this system stimulated robust humoral and cellular immune responses, demonstrating protective efficacy and a favorable safety profile in mouse models. This vaccine represents a promising candidate for protecting higher-risk individuals against severe COVID-19 and potentially reducing the incidence and severity of long COVID. The WNP system exhibits broad applicability for mRNA-based prevention and therapeutic applications.

MATERIALS AND METHODS

Cells and virus

HEK 293T (CRL-3216) cells were purchased from American Type Culture Collection (ATCC). BHK-21-hACE2 and Caco-2-N cells were maintained in Yu Chen's lab. They were cultured in Dulbecco's Modified Eagle Medium (Gibco, United States) supplemented with 10% fetal bovine serum (Lonsera, China) and 1% penicillin/streptomycin (Gibco, United States) at 37 °C with 5% CO_2. Omicron BA.1 strain (HB0000428) was provided by Hubei Provincial Center for Disease Control and Prevention.

Animal experiments

Mouse experiments conducted under specific pathogen-free conditions were performed at the Animal Experimentation Centre of Wuhan University. Infectivity experiments were performed at the Animal Biosafety Level-III (ABSL-III) Laboratory facility.

The study design was not blinded, and animals were randomly assigned to each group. Female BALB/c mice were subjected to a 12-h

night-day cycle at a constant room temperature (22 ± 2 °C, 45%–65% relative humidity) in pathogen-free conditions. Prior to vaccinations, IVIS imaging, blood collection from the posterior orbital venous plexus, viral infection and euthanasia, mice were anesthetized using continuous nasal inhalation of isoflurane at concentrations between 2% and 4%. Toe pinch was used to determine that the mice had lost consciousness. For collecting the tissues of mice in specific pathogen-free conditions, they were euthanized by cardiac blood collection under anesthesia, and the collections in infective experiments were conducted after euthanasia by cervical dislocation.

RNA synthesis

The templates encoding the signal peptide-RBD(M5)-hFc or luciferase, which include T7 promoter, 5′UTR, 3′UTR and poly A tail were purified using phenol chloroform extraction and subsequently were transcribed into mRNA by T7 RNA polymerase (Kactus, China). In the production of modified mRNA, uridine-5′-triphosphate was substituted with N1-methylpseudouridine 5′-triphosphate (Syngene, China). The mRNA was then precipitated with lithium chloride. Following this, the mRNA was capped using vaccinia capping enzyme and 2′-O-Methyltransferase (Yeasen, China) and purified through the same method.

Lipid nanoparticle (LNP) encapsulation of the mRNA and characterization

For the ethanol phase, the SM-102 and MC3 systems were provided by Yin Hao's group at the Institute of Medical Sciences, Wuhan University, while the WNP system was obtained through a thorough mixing of storage solutions containing ionizable lipids, neutral lipids, cholesterol and PEG lipids (Sinopeg, China) in a specified ratio. The mRNA was diluted in a 20 mM sodium acetate buffer solution (Coolaber, China) at pH 4 and served as the aqueous phase. Afterwards, the chip was inserted into the microfluidic instrument INano™ L + Myano (Micro & Nano, China). The ethanol and aqueous phases were aspirated using a syringe and mounted onto the injection port of the chip respectively. The total flow rate of the injections was configured to 12 mL/min using the microfluidic controller software, with a flow rate ratio of ethanol phase to aqueous phase set at 2:3. A sodium acetate buffer solution at pH 5 was utilized in the SM-102 system, while the MC3 system employed a sodium acetate buffer solution at pH 4. The flow rate ratio of these two systems was set at 1:3. Following the activation of the equipment, the effluent was collected. Subsequently, the sodium acetate buffer and ethanol were replaced with PBS (pH 7.4) using a 100 kDa ultrafiltration centrifuge tube (Millipore, United States). The samples were then filtered through a 0.22 μm filter membrane and stored at 4 °C. The hydrated particle size and zeta potential were measured using a nanoparticle size analyzer (OMEC, China). The samples were assessed using Ribogreen dye (Invitrogen, United States) to determine free and total RNA concentrations, after which the actual packed RNA concentration was calculated.

Luciferase transfection *in vitro*

HEK 293T cells were seeded on 48-well plates and incubated for approximately 18 h until they reached 60%–70% confluence. Firefly luciferase mRNA was packaged and the LNP was diluted to an RNA concentration of 10 μg/mL. Then 0.025 mL of luc-LNP was added to each well. 24 h after transfection, cells were harvested in passive lysis buffer for measuring relative luciferase activity using the luciferase assay system (Vazyme, China).

Luciferase transfection *in vivo*

Luc-LNP (0.1 mL) was intramuscularly injected into female C57BL/6 mice aged 6–7 weeks. The ventral surface hair of the mice was removed and luciferase potassium salt (Yeasen) was intraperitoneally injected at a dosage of 150 mg/kg at 6 h, 24 h, and 48 h post-injection. The mice were anesthetized with isoflurane during measurement. Two mice from each group were anesthetized with isoflurane and dissected at 6 h post-injection to detect luminescent signals in the muscle, liver and spleen. Mice injected with a placebo were employed as a negative control. The luminous flux was measured using the IVIS Spectrum (PerkinElmer, United States).

mRNA transfection

The RBD(M5)-hFc mRNA was transfected into HEK 293T cells using Lipofectamine™2000 (Thermo Fisher Scientific, United States). After 48 h, the supernatant was collected and isolated by centrifugation at 1000 ×*g*, followed by concentration in a 10 kDa ultrafiltration centrifuge tube (Millipore) at 2000 ×*g*. Then the samples were mixed with 5 × SDS non-reducing loading buffer (without reducing agents such as DTT and 2-mercaptoethanol). Subsequently, the samples were loaded directly without heating for SDS-PAGE performed on 4.5% stacking gel and 10% resolving gel (Epizyme Biotech, China). The RBD protein was detected by Western blotting using a mouse monoclonal antibody against RBD (Sino Biological, China, 1:1000).

Safety evaluation

RBD(M5)-hFc mRNA was packaged, and the LNP was diluted to an RNA concentration of 10 μg/mL. A volume of 0.1 mL either LNP or PBS was intramuscularly injected into 6–7 weeks old female BALB/c mice under anesthesia with isoflurane on days 0 and day 14. Blood samples were collected 7 days prior to the injections and 8 h after each injection when the mice were anesthetized with isoflurane. The serum was separated and analyzed using the Alanine Aminotransferase (ALT/GPT) Activity Assay Kit (Elabscience, China) to assess the changes in ALT activity. 8 h following the second injection, the mice were anesthetized with isoflurane and then euthanized by cervical dislocation. Their livers and muscles were collected and stained with H&E for histological sectioning (Pinuofei, China). Total RNA from the livers was isolated (Vazyme), and the relative mRNA levels of the pro-inflammatory cytokines *Il1b*, *Tnfa* and *Il6* were quantified by qPCR, using *Gapdh* (Supplementary Table S1) as the internal reference gene after reverse transcription (Vazyme).

Mouse vaccination

RBD(M5)-hFc mRNA was packaged, and the LNP was diluted to an RNA concentration of 10 μg/mL. A volume of 0.1 mL of either LNP or PBS was intramuscularly injected into 6–7 weeks old female BALB/c mice on day 0 and day 14 under anesthesia with isoflurane. Blood samples were collected on day 14 and day 28 when the mice were anesthetized with isoflurane for the detection of the RBD(WT)-specific IgG antibodies, and the samples collected on day 28 were also tested for neutralizing antibody potency using pseudovirus.

Enzyme-linked immunosorbent assay (ELISA)

Each well of the ELISA plate (Corning, United States) was coated with 3 μg of RBD(WT)-His protein which was diluted in 0.1 M carbonate inclusion buffer (pH 9.6). The plates were laid flat overnight at 4 °C in a humidified environment. Subsequently, the plates were washed three times with PBS containing 0.05% Tween. The plates were then blocked for 2 h at 37 °C using 1% BSA in PBS. Following this, a 100-fold dilution of the sera in the blocking solution was added, and the plates were incubated at 37 °C for 2 h followed by five washes. Goat anti-Mouse IgG (H + L), human ads-AP (Southern Biotech, United States), diluted in the blocking solution, was added to the plates, which were then incubated at 37 °C for 1 h. After an additional five washes, *p*-nitrophenyl phosphate (Sigma Aldrich, United States) mixed with Tris-HCl buffer was added

and the plates were incubated at room temperature for 1 h, protected from light. The optical density at 405 nm was measured by a Spectra MaxiD3 (Molecular Devices, United States).

SARS-CoV-2 pseudoviruses neutralization assay

The entire system was provided by Yan Huan's research group. BHK21-hACE2 cells were seeded in 10 cm dishes and incubated for approximately 24 h until they reached 90%–100% confluence. To inactivate complement, mouse sera were incubated at 55 °C for 30 min. Subsequently, 25 μL of 25-fold diluted serum was added to each well, and 25 μL of DMEM was added to the positive control well. Pseudovirus BA.1, BA.5.2, BF.7, BQ.1.1, XBB.1.5, EG.5.2, JN.1 and KP.3 were diluted to a $TCID_{50}$ of 5000, and 25 μL of each diluted pseudovirus was added respectively. The sera and pseudoviruses were incubated for 30 min at 37 °C, after which 50 μL of resuspended cells was added. The mixture was then incubated for 16 h. Following this incubation, the supernatant was removed, and the Bright-Glo™ luciferase assay system (Promega, United States) was added. The plates were then incubated at room temperature in the dark for 2 min. Next, they were placed into the Varioskan LUX (Thermo Fisher Scientific) for oscillation for 2 min, and the intensity of luminescence was detected. The inhibition rate was calculated based on the positive control.

Flow cytometry analyses

To detect the level of cellular immunity stimulated by vaccines, the BALB/c mice were anesthetized with isoflurane and then euthanized by cervical dislocation on day 42 to collect spleens and isolate splenocytes. RBD(BA.2)-His protein was added to 1×10^7 splenocytes at a concentration of 5 μg/mL. The splenocytes were stimulated for 17 h. Subsequently, Brefeldin A was added at a final concentration of 5 ng/mL, and the cells were incubated for an additional 5 h. Following this, the cells were collected and washed with 0.5% BSA in PBS prior to surface antibody staining. The staining mix included CD3 (PC5.5) (BD Biosciences, United States), CD4 (FITC) (BioLegend, United States), and CD8 (APC) (BioLegend). After a 30-min incubation on ice, the cells were fixed, permeabilized, and stained for intracellular cytokines. The staining mix contained IFN-γ (PE) (BioLegend), IL-2 (BV421) (BioLegend), IL-4 (BV421) (BioLegend), and IL-5 (PE) (BioLegend). Following another 30-min incubation on ice, the cells were washed, resuspended, filtered through a 200-mesh sieve, and analyzed using a CytoFlex flow cytometer (Beckman Coulter, United States). Data were analyzed with FlowJo software (Supplementary Fig. S2).

Challenge experiment

To assess protective efficacy, the BALB/c mice were anesthetized with isoflurane and then infected with 43,500 PFU of Omicron BA.1 via nasal drip in week 5. They were euthanized by cardiac blood collection under anesthesia with isoflurane after four days post infection and lung tissues were collected. The left lungs were stained with H&E for histological sectioning (Pinuofei, China), while RNA was extracted from the right lungs and reverse transcribed into cDNA (Takara, Japan). The copy numbers of the *N* and *E* genes of SARS-CoV-2 (Supplementary Table S1) were detected using qPCR (Yeasen).

Replicon delivery particles (RDPs) inhibition experiment

Caco-2-N cells were plated on a 48-well plate with a density of 2.5×10^5 cells per well. The diluted serum was incubated with XBB.1.5-ΔN-GFP RDPs (MOI = 0.01) for 1 h at 37 °C prior to infection. At 36 h post-infection, the plate was observed under a fluorescence microscope. Then the RNA was extracted from the cells and reverse transcribed into cDNA (Vazyme). The relative RNA expression of the *E* gene of SARS-CoV-2 was detected using qPCR (Yeasen) and normalized to *GAPDH* (Table S1).

Statistical analysis

Statistical analysis was mainly processed using GraphPad Prism 8.0. Unless otherwise specified, data are presented as mean ± SEM in all experiments. One-way ANOVA with multiple comparisons tests and the Kruskal-Wallis test with Dunnett T3 post-test were employed to assess statistical significance among different groups (ns, not significant, $^*P < 0.05$, $^{**}P < 0.01$, $^{***}P < 0.001$, $^{****}P < 0.0001$).

DATA AVAILABILITY

All data relevant to the study are included in the article or uploaded as supplementary information.

ETHICS STATEMENT

Animal studies were carried out in accordance with the recommendations in the guide for the Care and Use of Laboratory Animals of the National Institutes of Health. The protocol was approved by the Institutional Animal Care and Use Committee at Wuhan University (AUP: WP20220044). All SARS-CoV-2 authentic virus-related experiments (S01322040G) were approved by the Institutional Biosafety Committee (IBC) of ABSL-III Laboratory at Wuhan University and all samples were inactivated and removed according to standard procedures approved by the IBC.

AUTHOR CONTRIBUTIONS

Weiyi Yu: conceptualization (equal), methodology (lead), validation (lead), formal analysis (lead), investigation (lead), writing-original draft (lead) and visualization (lead). Xianying Chen: methodology (lead) and investigation (equal). Qiubing Chen: methodology (equal) and investigation (supporting). Peixuan Chen: investigation (equal). Naizhang Liu: investigation (equal). Yingjian Li: methodology (equal) and investigation (equal). Xue Tan: investigation (supporting). Qiuhan Zhang: investigation (supporting). Yan Rao: investigation (supporting). Ming Guo: investigation (supporting). Zhixiang Huang: investigation (supporting). Xin Wang: investigation (supporting). Zhen Zhang: methodology (supporting), investigation (supporting) and funding acquisition (supporting). Wenjie Xiang: investigation (supporting). Yuzhen Zhang: investigation (supporting). Qianyun Liu: methodology (supporting) and funding acquisition (supporting). Hao Yin: resources (supporting). Li Zhou: methodology (supporting), resources (supporting), writing-review & editing (lead), supervision (equal) and funding acquisition (equal). Yu Chen: conceptualization (equal), resources (equal), writing-review & editing (equal), supervision (equal) and funding acquisition (lead). Ke Lan: conceptualization (lead), resources (lead), writing-review & editing (supporting) and project administration (lead).

CONFLICT OF INTEREST

The authors declare that they have no competing interests. Prof. Ke Lan is an editorial board member for *Virologica Sinica* and was not involved in the editorial review or the decision to publish this article.

ACKNOWLEDGMENTS

This work was supported by the National Key R&D Program of China (2021YFF0702000 to Y.Chen, 2021YFC2300700 to L.Zhou), the National Natural Science Foundation of China (grants 82341061, 82172243 and 82372223 to Y.Chen), the Fundamental Research Funds for the Central Universities (2042022dx0003 to Y.Chen), the Hubei Provincial Natural Science Foundation (2023AFB201 to Z.Zhang, and 2024AFB906 to L.Zhou.), and the China Postdoctoral Science Foundation (2023M732705 to Q.Liu).

APPENDIX A. SUPPLEMENTARY DATA

Supplementary data to this article can be found online at https://doi.org/10.1016/j.virs.2025.09.001.

REFERENCES

Aguilar-Bretones, M., Fouchier, R.A., Koopmans, M.P., Van Nierop, G.P., 2023. Impact of antigenic evolution and original antigenic sin on SARS-CoV-2 immunity. J. Clin. Investig. 133, e162192.

Ai, L., Li, Y., Zhou, L., Yao, W., Zhang, H., Hu, Z., Han, J., Wang, W., Wu, J., Xu, P., et al., 2023. Lyophilized mRNA-lipid nanoparticle vaccines with long-term stability and high antigenicity against SARS-CoV-2. Cell Discov 9, 9.

Ali, S., Smaby, J.M., Momsen, M.M., Brockman, H.L., Brown, R.E., 1998. Acyl chain-length asymmetry alters the interfacial elastic interactions of phosphatidylcholines. Biophys. J. 74, 338–348.

Cao, Y., Jian, F., Wang, J., Yu, Y., Song, W., Yisimayi, A., Wang, J., An, R., Chen, X., Zhang, N., et al., 2023. Imprinted SARS-CoV-2 humoral immunity induces convergent omicron RBD evolution. Nature 614, 521–529.

Carrasco, M.J., Alishetty, S., Alameh, M.G., Said, H., Wright, L., Paige, M., Soliman, O., Weissman, D., Cleveland, T.E.T., Grishaev, A., Buschmann, M.D., 2021. Ionization and structural properties of mRNA lipid nanoparticles influence expression in intramuscular and intravascular administration. Commun. Biol. 4, 956.

Chen, J., Xu, Y., Zhou, M., Xu, S., Varley, A.J., Golubovic, A., Lu, R.X.Z., Wang, K.C., Yeganeh, M., Vosoughi, D., Li, B., 2023. Combinatorial design of ionizable lipid nanoparticles for muscle-selective mRNA delivery with minimized off-target effects. Proc. Natl. Acad. Sci. U. S. A. 120, e2309472120.

Chen, Y, Liu, Q, Guo, D, 2020. Emerging coronaviruses: Genome structure, replication, and pathogenesis. J Med Virol 92, 418–423.

Chen, L., Liu, W., Zhang, Q., Xu, K., Ye, G., Wu, W., Sun, Z., Liu, F., Wu, K., Zhong, B., Mei, Y., Zhang, W., Chen, Y., Li, Y., Shi, M., Lan, K., Liu, Y., 2020. RNA based mNGS approach identifies a novel human coronavirus from two individual pneumonia cases in 2019 wuhan outbreak. Emerg. Microb. Infect. 9, 313–319.

Chen, Y., Liu, Q., Guo, D., 2020b. Emerging coronaviruses: genome structure, replication, and pathogenesis. J. Med. Virol. 92, 418–423.

Chen, Y., Liu, Q., Zhou, L., Zhou, Y., Yan, H., Lan, K., 2022. Emerging SARS-CoV-2 variants: why, how, and what's next? Cell Insight 1, 100029.

Dipiazza, A.T., Leist, S.R., Abiona, O.M., Moliva, J.I., Werner, A., Minai, M., Nagata, B. M., Bock, K.W., Phung, E., Schäfer, A., et al., 2021. COVID-19 vaccine mRNA-1273 elicits a protective immune profile in mice that is not associated with vaccine-enhanced disease upon SARS-CoV-2 challenge. Immunity 54, 1869–1882.e1866.

Fu, J., Wu, S., Bao, N., Wu, L., Qu, H., Wang, Z., Dong, H., Wu, J., Jin, Y., 2025. A universal strategy of anti-tumor mRNA vaccine by harnessing "Off-the-Shelf" immunity. Adv. Sci. (Weinh.) 12, e2401287.

Hassett, K.J., Benenato, K.E., Jacquinet, E., Lee, A., Woods, A., Yuzhakov, O., Himansu, S., Deterling, J., Geilich, B.M., Ketova, T., Mihai, C., Lynn, A., Mcfadyen, I., Moore, M.J., Senn, J.J., Stanton, M.G., Almarsson, Ö., Ciaramella, G., Brito, L.A., 2019. Optimization of lipid nanoparticles for intramuscular administration of mRNA vaccines. Mol. Ther. Nucleic Acids 15, 1–11.

Kapoor, K., Chen, T., Tajkhorshid, E., 2022. Posttranslational modifications optimize the ability of SARS-CoV-2 spike for effective interaction with host cell receptors. Proc. Natl. Acad. Sci. U. S. A. 119, e2119761119.

Kim, J.H., Chae, H.B., Woo, S., Song, M.S., Kim, H.J., Woo, C.G., 2023. Clinicopathological characteristics of autoimmune-like hepatitis induced by COVID-19 mRNA vaccine (Pfizer-BioNTech, BNT162b2): a case report and literature review. Int. J. Surg. Pathol. 31, 1156–1162.

Klein, N.P., Lewis, N., Goddard, K., Fireman, B., Zerbo, O., Hanson, K.E., Donahue, J.G., Kharbanda, E.O., Naleway, A., Nelson, J.C., Xu, S., Yih, W.K., Glanz, J.M., Williams, J.T.B., Hambidge, S.J., Lewin, B.J., Shimabukuro, T.T., Destefano, F., Weintraub, E.S., 2021. Surveillance for adverse events after COVID-19 mRNA vaccination. JAMA 326, 1390–1399.

Lan, Q., Yan, Y., Zhang, G., Xia, S., Zhou, J., Lu, L., Jiang, S., 2024. Clinical development of antivirals against SARS-CoV-2 and its variants. Curr. Res. Microb. Sci. 6, 100208.

Li, Y., Tan, X., Deng, J., Liu, X., Liu, Q., Zhang, Z., Huang, X., Shen, C., Xu, K., Zhou, L., Chen, Y., 2024. An optimized high-throughput SARS-CoV-2 dual reporter trans-complementation system for antiviral screening in vitro and in vivo. Virol. Sin. 39, 447–458.

Liu, Q., Zhao, H., Li, Z., Zhang, Z., Huang, R., Gu, M., Zhuang, K., Xiong, Q., Chen, X., Yu, W., et al., 2023. Broadly neutralizing antibodies derived from the earliest COVID-19 convalescents protect mice from SARS-CoV-2 variants challenge. Signal Transduct. Targeted Ther. 8, 347.

Lok, L.S.C., Sarkar, S., Lam, C.C.I., Law, C.F., Chau, S.T., Leung, C.Y.T., Cheang, W.H., Li, T., Monteiro, O., Baptista-Hon, D.T., 2024. Long COVID Across SARS-CoV-2 Variants: Clinical Features, Pathogenesis, and Future Directions, vol. 3, e70004.

Ma, C., Chen, X., Mei, F., Xiong, Q., Liu, Q., Dong, L., Liu, C., Zou, W., Zhan, F., Hu, B., et al., 2022. Drastic decline in sera neutralization against SARS-CoV-2 omicron variant in wuhan COVID-19 convalescents. Emerg. Microb. Infect. 11, 567–572.

Meo, S.A., Bukhari, I.A., Akram, J., Meo, A.S., Klonoff, D.C., 2021. COVID-19 vaccines: comparison of biological, pharmacological characteristics and adverse effects of Pfizer/BioNTech and moderna vaccines. Eur. Rev. Med. Pharmacol. Sci. 25, 1663–1669.

Paunovska, K., Loughrey, D., Dahlman, J.E., 2022. Drug delivery systems for RNA therapeutics. Nat. Rev. Genet. 23, 265–280.

Shi, Y., 2020. New virus, new challenge. Innovation 1, 100005.

Sun, S., He, L., Zhao, Z., Gu, H., Fang, X., Wang, T., Yang, X., Chen, S., Deng, Y., Li, J., et al., 2021. Recombinant vaccine containing an RBD-Fc fusion induced protection against SARS-CoV-2 in nonhuman primates and mice. Cell. Mol. Immunol. 18, 1070–1073.

Tanaka, H., Takata, N., Sakurai, Y., Yoshida, T., Inoue, T., Tamagawa, S., Nakai, Y., Tange, K., Yoshioka, H., Maeki, M., Tokeshi, M., Akita, H., 2021. Delivery of oligonucleotides using a self-degradable lipid-like material. Pharmaceutics 13, 544.

Vogel, A.B., Kanevsky, I., Che, Y., Swanson, K.A., Muik, A., Vormehr, M., Kranz, L.M., Walzer, K.C., Hein, S., Güler, A., et al., 2021. BNT162b vaccines protect rhesus macaques from SARS-CoV-2. Nature 592, 283–289.

Wrapp, D., Wang, N., Corbett, K.S., Goldsmith, J.A., Hsieh, C.L., Abiona, O., Graham, B. S., Mclellan, J.S., 2020. Cryo-EM structure of the 2019-nCoV spike in the prefusion conformation. Science 367, 1260–1263.

Wu, Y., Wang, S., Zhang, Y., Yuan, L., Zheng, Q., Wei, M., Shi, Y., Wang, Z., Ma, J., Wang, K., et al., 2022. Lineage-mosaic and mutation-patched spike proteins for broad-spectrum COVID-19 vaccine. Cell Host Microbe 30, 1732–1744.e1737.

Ying, B., Scheaffer, S.M., Whitener, B., Liang, C.Y., Dmytrenko, O., Mackin, S., Wu, K., Lee, D., Avena, L.E., Chong, Z., et al., 2022. Boosting with variant-matched or historical mRNA vaccines protects against Omicron infection in mice. Cell 185, 1572–1587.e1511.

Yisimayi, A., Song, W., Wang, J., Jian, F., Yu, Y., Chen, X., Xu, Y., Yang, S., Niu, X., Xiao, T., et al., 2024. Repeated Omicron exposures override ancestral SARS-CoV-2 immune imprinting. Nature 625, 148–156.

Zatsepin, T.S., Kotelevtsev, Y.V., Koteliansky, V., 2016. Lipid nanoparticles for targeted siRNA delivery - going from bench to bedside. Int. J. Nanomed. 11, 3077–3086.

Zhang, G., Wang, Q., Ji, K., Wang, Y., Xu, W., Zhou, J., Liu, Z., Xiu, R., Xing, L., Zhou, J., Shi, Y., Lu, X., Wang, X., Ying, B., Lu, L., Jiang, S., 2025. Leveraged vaccination to alleviate original antigenic sin for enhancing broad-neutralizing antibody response against SARS-CoV-2 omicron subvariants. MedComm 6, e70273, 2020.

Zhang, H., Shi, S., Sun, L., Li, S., Zhang, Y., Li, Z., Hou, J., Li, P., Shen, J., Cheng, X., Jiang, S., Gao, Z., Wang, X., Jiang, X., Xia, B., 2025. Screening and discovery of an antiviral candidate inhibiting the SARS-CoV-2 envelope (2-E) channel. Curr. Res. Microb. Sci. 9, 100409.

Zhang, N.N., Li, X.F., Deng, Y.Q., Zhao, H., Huang, Y.J., Yang, G., Huang, W.J., Gao, P., Zhou, C., Zhang, R.R., et al., 2020b. A thermostable mRNA vaccine against COVID-19. Cell 182, 1271–1283.e1216.

Zhao, Y., Ni, W., Liang, S., Dong, L., Xiang, M., Cai, Z., Niu, D., Zhang, Q., Wang, D., Zheng, Y., et al., 2023. Vaccination with S(pan), an antigen guided by SARS-CoV-2 S protein evolution, protects against challenge with viral variants in mice. Sci. Transl. Med. 15, eabo3332.

Zheng, X., Liu, B., Ni, P., Cai, L., Shi, X., Ke, Z., Zhang, S., Hu, B., Yang, B., Xu, Y., et al., 2025. Development and application of an uncapped mRNA platform. Ann. Med. 57, 2437046.

Zhou, P., Yang, X.L., Wang, X.G., Hu, B., Zhang, L., Zhang, W., Si, H.R., Zhu, Y., Li, B., Huang, C.L., et al., 2020. A pneumonia outbreak associated with a new coronavirus of probable bat origin. Nature 579, 270–273.

Zhu, N., Zhang, D., Wang, W., Li, X., Yang, B., Song, J., Zhao, X., Huang, B., Shi, W., Lu, R., Niu, P., Zhan, F., Ma, X., Wang, D., Xu, W., Wu, G., Gao, G.F., Tan, W., 2020. A novel coronavirus from patients with pneumonia in China, 2019. N. Engl. J. Med. 382, 727–733.